

## Research Paper

# Fault Diagnosis of Induction Motors: An Architecture for Real-Time Assessment as a Cyber-Physical System

Ranjan Sasti Charan PAL\*, Nagesh DEWANGAN, Amiya Ranjan MOHANTY

*Department of Mechanical Engineering, Indian Institute of Technology  
Kharagpur 721302, India*

\*Corresponding Author e-mail: ranjan\_pal@iitkgp.ac.in

Induction motors (IMs) have a crucial and significant role in various industrial sectors. With the prolonged operation of IMs, faults tend to develop that can be classified into five major categories, i.e., broken rotor bars, stator winding faults, air-gap eccentricity, bearing faults, and load torque fluctuations. If the faults go undetected, it may lead to catastrophic failure. Hence, the predictive-based condition monitoring technique has evolved as a real-time fault diagnosis that exploits the revolutionary idea of cyber-physical system (CPS). Furthermore, motor current signature analysis (MCSA) is a non-invasive fault diagnosis technique of a motor that can be used to investigate the presence of five fault types. However, the major constraint that industries face today is the on-field implementation of MCSA-based fault diagnosis involving CPS-based architecture, executed in an automated manner. Hence, the present article depicts algorithms that aim at real-time monitoring of IMs through a CPS framework. The proposed methodology is automated, does not involve any human intervention, and has been validated with real-time experiments, depicting its effectiveness and practicality.

**Keywords:** cyber-physical system; fault diagnosis; induction motors; motor current signature analysis.

## 1. INTRODUCTION

The industrial and commercial sectors mainly depend on induction motors (IMs) as major prime movers for running equipment due to their robust structure, simplicity, and efficiency [1]. However, with continuous usage, the occurrence of faults in IMs is inevitable. An unexpected appearance of fault, if left undetected, leads to production loss and catastrophic events that can take a toll on the lives of plant personnel [2, 3]. Thus, to increase the reliability of the machines and maintain machine uptime, it is of utmost importance to implement real-time monitoring of motor health condition via a framework involving a cyber-physical system (CPS) [4–6]. The IM is connected to the internet by

means of a sensor to measure the physical parameters such as current, temperature, vibration, voltage, etc. The measured parameter is then analyzed to scrutinize the motor health status and develop an effective maintenance schedule. The computational resources and motor interlink using standard internet protocols for real-time monitoring.

GROUNDAR *et al.* [7] used a temperature sensor (thermistor), accelerometer (MEAS), and microcontroller (Waspnote PRO) to record temperature and acceleration data from a motor. The recorded physical parameters (temperature/acceleration data) were transferred to the Esri cloud computing platform. The Waspnote PRO was able to maintain the maximum sampling frequency ( $F_s$ ) of 1 kHz. The fast Fourier transform (FFT) of the acceleration data was computed to investigate the vibration spectrum wherein the frequency range was observed till 500 Hz.

A CPS-based condition monitoring technique for motors was presented by CIVERCHIA *et al.* [8]. Standard internet protocols (IPs) were used viz. IEEE 802.15.4, 6LoWPAN (IPv6 over Low Power Wireless Personal Area Networks), and CoAP (Constrained Application Protocol) for data transmission between the transducers and a microcontroller (CC2538). The link layer was managed by IEEE 802.15.4, the network layer is aided by 6LoWPAN and the application layer is organized by CoAP. The vibration data of the machine was captured by a microcontroller (CC2538), where  $F_s$  is set at 800 Hz. The machine health status was inspected by tracking the change in the RMS (root mean square) value of vibration data.

WU *et al.* [9] ventured into the implementation of wireless sensors, machine learning, and cloud computing. A pump driven by a motor was used for experimental analysis from which the current and vibration data were measured using a tri-axial accelerometer and a current sensor (CTRS 501). The analog signal was received by the microcontroller (Arduino), which converts the analog to a digital signal. The digital signal is then communicated to the Predix computing platform via the ZigBee module. However, the technique involved in the fault detection of the machine was omitted.

A microcontroller (myRIO-1900) and a vibration sensor (ADXL345) were used by GANGA and RAMACHANDRAN [10] to record vibration data. A serial device interface was used to transfer the recorded vibration signal to SIMATIC IoT2040 Gateway. The vibration amplitude was monitored at different time periods. The microcontroller (myRIO-1900) can attain a maximum  $F_s$  value of 800 Hz.

A Raspberry Pi coupled with a MEMS (micro-electro-mechanical system) sensor was maneuvered to capture vibration data from a pump driven by a motor, as presented by JUNG *et al.* [11]. The RMS value of vibration data and the power spectral density (PSD) were examined to ascertain the vibration level in

the pump. The frequency resolution of the PSD was compromised since the data was recorded for a time duration of 0.25 s.

A methodology involving fog layer architecture for real-time predictive maintenance of motors was presented by XENAKIS *et al.* [12]. The RMS, crest factor, and kurtosis values of the vibration data were evaluated to investigate the motor vibration levels. However, the technique discussed was not corroborated with real-time experimentations.

MAGADÁN *et al.* [13] utilized a temperature sensor (HDC1000) and an accelerometer (MPU9250) that aided in recording temperature and vibration data through a microcontroller (Raspberry Pi 3 Model B+). The maximum value of  $F_s$  was set at 1 kHz. The temperature and vibration data were then conveyed to the ThingSpeak analytics platform for motor analysis. The vibration spectrum was analyzed for any abnormalities by scrutinizing spectrum data until 500 Hz.

The vibration data of a motor was collected by adopting a piezoelectric sensor, as cited by FIRMANSAH *et al.* [14]. The process was guided by using a microcontroller (NodeMCU) that later communicated the vibration data to the cloud using a router. However, the methodology involved in motor fault diagnosis and the value of  $F_s$  to record the data were not presented.

KUNTHONG *et al.* [15] used ADXL345, ACS712, and DS18B20 to record vibration, current, and temperature parameters for motor health diagnosis. A microcontroller (ESP8266) was positioned to interface the sensor data into Node-Red cloud-based platform. The motor fault was detected by monitoring any abrupt change in the waveform of the time-stamp signal.

A temperature sensor (LM35) and a current sensor (ACS712) were used to record the physical parameters of the motor for condition monitoring, as shown by CHOUDHARY *et al.* [16]. The sensor data was acquired using a microcontroller (Arduino), next transmitted to the Cayenne analytics platform for the data post-processing. The computational analysis was done in Cayenne, and the RMS values of the measured signals were monitored. If the RMS value of the measured signal overshooted the threshold value, a signal was sent to the microcontroller, which then communicated a command to the relay to disengage the motor from the power supply.

A microcontroller accompanied by a current sensor (ACS712) was installed to record the current data, as presented by KHAN *et al.* [17]. The current data was then transferred to the ThingSpeak server for further analysis. The RMS value of current data was measured and thus the motor health status was assessed.

A potential transformer, a current sensor (ACS712) and a temperature sensor (LM35) were implemented to record voltage, current, and temperature data, as presented by ASHMITHA *et al.* [18]. The data recording was aided by a microcontroller (Arduino) and sent to the ThingSpeak website, where the RMS

values of the recorded data were calculated. If the RMS value detected showed abnormal behaviors, then the microcontroller sent a feedback signal to the relay, and the motor functioning was terminated to avoid further loss.

STM32 microcontroller was used by ZHANG and KANG [19], which helped in obliterating the purpose of using a central processing unit (CPU) to connect the input/output peripherals of sensors and the microcontroller. The vibration data were recorded by using a vibration sensor (MMA7455L) by maintaining the value of  $F_s$  at 5 kHz from a rotating machine by deploying direct memory access (DMA). However, latency in recording the data was created with DMA usage since the packets of data were recorded consecutively. Thus, a time delay of a few milliseconds led to erroneous results in recording the data. Microcontrollers that work on embedded systems form the foundation for data acquisition. The general-purpose input/output (GPIO) pins present on the microcontroller and the input/output peripherals of the ADC (analog to digital converter) module interact with each other by the operating system (OS) of the microcontroller. The OS reads and writes the data in the peripheral's register (or memory) at every time step. As a result, random jitters start appearing at the core of the OS of the microcontroller when the  $F_s$  is set above 500 Hz. Furthermore, faults occurring in IMs can be divided into five major categories viz. broken rotor bars, stator winding faults, air-gap eccentricity, bearing faults, and load torque fluctuations [20–26]. The research work that makes use of microcontroller as prescribed in the literature does not classify the five fault types. Motor current signature analysis (MCSA) is a potential non-invasive fault diagnostic methodology [27–29] that is used to differentiate the five fault types by interpreting the characteristic fault frequencies (CFFs) [30, 31] in the motor current spectrum observed in the frequency range of 0–5 kHz [32–34]. Hence, the Nyquist sampling frequency, for current data acquisition, should be at least 10 kHz. Thus, due to random jitters in microcontrollers, the motor fault diagnosis using MCSA is infeasible.

The objective of the present work is to implement CPS-based fault diagnostic strategy of motors using MCSA to scrutinize the five fault types, without any human intervention, by using an industrial mini-computer (IMC). The  $F_s$  of the data acquisition (DAQ) system is set at 10 kHz, and the current data is transferred to IMC across a wireless network. Furthermore, the IMC is used to process the current data and detect the presence of the five types of faults. The motor health status is recorded as a Boolean value of 1 when a fault is present, and the value is 0 when the fault does not occur. The Boolean value, along with the corresponding current spectrum data, is stored in two separate CSV (comma-separated values) files, which are then transferred to Google Cloud Storage (GCS) form, where the plant personnel can assess the files and chalk out the maintenance schedules.

This paper is organized as follows: Sec. 2 deals with an explanation of the proposed CPS based framework for fault diagnosis. It focuses on the process flow and algorithm developed for real-time fault diagnosis of IMs. Section 3 demonstrates the experimental test setup. The results are discussed in Sec. 4, and the conclusions are presented in Sec. 5.

## 2. PROPOSED ARCHITECTURE FOR CPS-BASED REAL-TIME FAULT DIAGNOSIS OF IMs

CPS is a strategic approach that involves interlinking the physical component, i.e., IM with the internet to track the real-time condition of the motor, as reported by HUMAYED *et al.* [35]. The architecture for fault diagnosis proposed in the present paper is depicted in Fig. 1. The CPS framework consists of an induction motor, clamp-type current transducer (CT), DAQ compatible with the Wi-Fi module, IMC with Wi-Fi connectivity, and GCS.

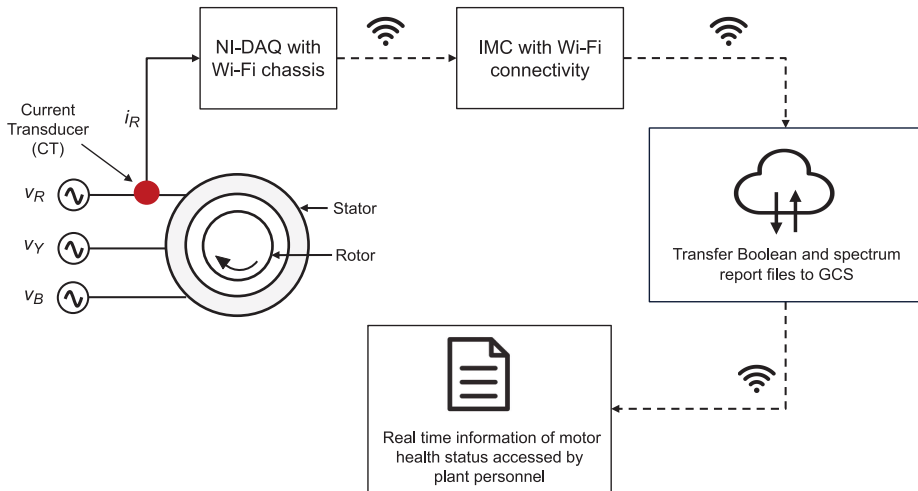


FIG. 1. Framework of the real-time CPS-based fault diagnosis of IMs by applying MCSA.

The Wi-Fi-based DAQ system demonstrates the feasibility to record current data and transfer it to IMC from any location across a wireless network. The DAQ unit is developed by National Instruments (NI) and involves a DAQ card NI 9215 C series voltage module and NI 9191 cDAQ chassis. Initially, the DAQ chassis is connected to the IMC through an Ethernet cable. The Wi-Fi network is enabled in the chassis using the Dynamic Host Configuration Protocol (DHCP). After successfully connecting the DAQ chassis with IMC across the Wi-Fi network, the Ethernet cable is removed. LabVIEW environment is used to record the current data in IMC as described in Algorithm 1. The procedure

---

**Algorithm 1.** Generate current time signal for 20 s in the LabVIEW environment.

---

1. Set the channel name of the DAQ card in LabVIEW.
  2. Specify the range as  $-10$  V to  $10$  V.
  3. Set the sensitivity of the channel as  $32.4$  mV/A.
  4. Set the sampling frequency ( $f_s$ ) as  $10$  kHz.
  5. Read the current signal ( $I$ ) for  $20$  s.
  6. Transfer the signal to IMC across a wireless network.
  7. Save the current signal in TDMS (technical data management streaming) file format.
- 

to acquire motor current data is presented in Fig. 2. The sampling frequency ( $F_s$ ) of each channel, the duration of the current data recorded ( $T$ ), the sensitivity of the sensor, and the voltage input range of the DAQ module, are set in the LabVIEW environment. The total number of data points ( $N$ ) recorded is expressed by Eq. (2.1)

$$(2.1) \quad N = T \cdot F_s.$$

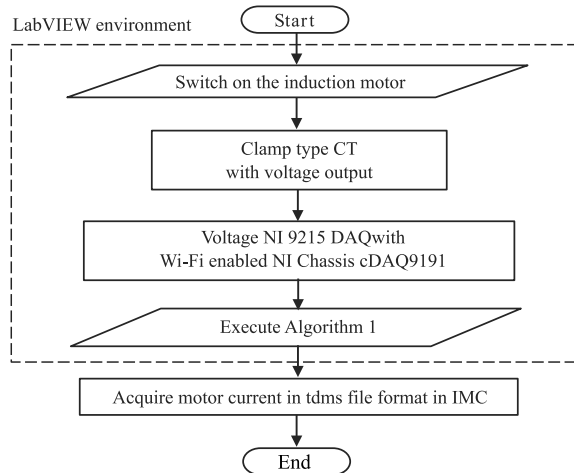


FIG. 2. Flowchart depicting procedure to acquire current data in IMC.

The fault diagnosis algorithm, developed in the Python environment, deals with encountering CFFs in the current spectrum array without any human intervention. While recording the motor current signal ( $I$ ), a constant bias may appear in the current signal since the DAQ module operates in “DC Coupling” mode. The corrected signal ( $I_{\text{corr}}$ ) is obtained by removing the bias, which is expressed by Eq. (2.2)

$$(2.2) \quad I_{\text{corr}} = I - I_{\text{mean}},$$

where  $I_{\text{mean}}$  is the mean value of  $I$ . The time domain signal  $I_{\text{corr}}$  is converted to the current spectrum by computing the absolute FFT in a linear scale. In order to enhance the dynamic range, the linear FFT is converted to a logarithmic scale by considering 1 A as the reference value. A Hanning window is applied to avoid the leakage effect and enhance the computation of spectral data as depicted in Algorithm 2a. The current spectrum value, i.e., frequency vs. current amplitude, is stored in a current array, forming an integral part of the Python workspace. Supply frequency and motor speed are detected based

**Algorithm 2a.** Calculation of the supply line frequency  $f_s$ .

1. Read the current signal ( $I$ ) from the TDMS file format that has been saved in IMC.
2. Calculate the mean value of  $I$  represented as  $I_{\text{mean}}$ .
3. Remove constant bias from  $I$  denoted as  $I_{\text{corr}} = I - I_{\text{mean}}$ .
4. Apply the Hanning window on  $I_{\text{corr}}$  denoted as  $I_{\text{Hann}}$ .
5. **if**  $T = 20$  s and  $F_s = 10$  kHz **then**
6.     Frequency resolution =  $df = 1/T = 0.05$  Hz.
7.     Number of data points in time signal =  $N = T \cdot F_s = 200\,000$  data points.
8.     Number of spectral lines =  $N_s = N/2 = 100\,000$  spectral lines.
9.     Compute the absolute FFT of  $I_{\text{Hann}}$  in logarithmic scale by considering 1 A as the reference, denoted by the current vector (CV), which is represented as:

$$\text{CV} = \left\{ 20 \log_{10} \left[ \frac{\frac{2}{N} |\text{FFT}(I_{\text{Hann}})|}{1} \right] \right\}_{100\,000 \times 1}.$$

10.     Create a frequency vector (FV) with  $df = 0.05$  Hz that is designated as:

$$\text{FV} = \{f\}_{100\,000 \times 1}.$$

11.     Create a 2D array designated by current spectrum (CS), which is denoted as:

$$\text{CS} = [\text{FV}, \text{CV}]_{100\,000 \times 2}.$$

12.     Locate the maximum value of amplitude in 2nd column of CS:

$$\text{Max\_CS} = \max[\text{CS}_{2\text{nd col}}].$$

13.     Supply line frequency ( $f_s$ ) is responsible for driving the induction motor. Hence,  $f_s$  has the highest amplitude in the current spectrum.  
         $\therefore f_s$  frequency value in  $[\text{CS}_{1\text{st col}}]$  corresponding to Max\_CS.

14. **else**

15.     Do not analyze the current time signal due to an insufficient number of data points in the current signal ( $I$ ).

on Algorithm 2a and Algorithm 2b, respectively. The CFFs [36–42] are then calculated by using Eqs. (2.3)–(2.6), that correspond to BRBs ( $f_{\text{BRBs}}$ ), stator

---

**Algorithm 2b.** Calculation of the motor speed  $f_m$ .

---

1. Calculate  $f_s$  from Algorithm 2a.

2. The actual synchronous speed ( $f_{\text{syn}}$ ) of the motor is given as:

$$f_{\text{syn}} = \frac{f_s}{p},$$

where  $p$  is the number of pole pairs.

3. The rated supply frequency ( $f_{s\_rat}$ ) and rated motor speed ( $f_{m\_rat}$ ) can be found on the motor nameplate.

$\therefore$  The rated synchronous speed of the motor is denoted as:  $f_{\text{syn\_rat}} = \frac{f_{s\_rat}}{p}$ ,

$\therefore$  Rated slip =  $s_{\text{rat}} = \frac{f_{\text{syn\_rat}} - f_{m\_rat}}{f_{\text{syn\_rat}}}$ .

4. Considering the load factor as 1.5, the maximum slip is determined as:

$$s_{\text{max}} = 1.5 \times s_{\text{rat}}.$$

5. Hence, the minimum speed the motor can attain is given as:

$$f_{m\_min} = (1 - s_{\text{max}}) \times f_{\text{syn}}.$$

6. Hence, the range of actual motor speed is represented as:

$$f_{m\_min} \leq f_m < f_{\text{syn}}.$$

7. In the CS array (from Algorithm 2a), peak frequencies can be established in the below frequency range:

- upper sideband range for motor speed (USBR\_MS):

$$(f_s + f_{m\_min}) \leq (f_s + f_m) < (f_s + f_{\text{syn}}),$$

- lower sideband range for motor speed (LSBR\_MS):

$$(f_s - f_{m\_min}) \geq (f_s - f_m) > (f_s - f_{\text{syn}}).$$

8. Locate the maximum value of amplitude in USBR\_MS and LSBR\_MS:

$$\text{Max\_USBR\_MS} = \max[\text{CS}_{2\text{nd col}}]_{\text{range: USBR\_MS}},$$

$$\text{Max\_LSBR\_MS} = \max[\text{CS}_{2\text{nd col}}]_{\text{range: LSBR\_MS}},$$

$$\therefore \text{Max\_MS} = \max[\text{Max\_LSBR\_MS}, \text{Max\_USBR\_MS}].$$

9.  $\therefore f_m =$  frequency value in  $[\text{CS}_{1\text{st col}}]$  corresponding to Max\_MS.

10. The actual motor slip ( $s$ ) that has been attained by the induction motor is denoted as:

$$s = \frac{f_{\text{syn}} - f_m}{f_{\text{syn}}}.$$


---

faults ( $f_{\text{SFs}}$ ), eccentricity ( $f_{\text{Fcc}}$ ), and bearing faults ( $f_{\text{Brg}}$ ) and are discussed in Algorithms 2c–2g:

$$(2.3) \quad f_{\text{BRBs}} = (1 \pm 2skf_s),$$

$$(2.4) \quad f_{\text{SFs}} = (2k + 1) f_s,$$

$$(2.5) \quad f_{\text{Ecc}} = f_s \pm f_m,$$

$$(2.6) \quad f_{\text{Brg}} = f_s \pm k f_{\text{Brg\_CFFs}},$$

where  $k = 1, 2, 3, \dots, f_s$  is the supply line frequency,  $f_m$  is the motor speed,  $f_{\text{Brg\_CFFs}}$  is one of the characteristic fault frequencies of the bearing viz. ball spin frequency, fundamental train frequency, ball pass frequency outer race, and ball spin frequency inner race. For Algorithm 2c, the threshold value of BRBs is  $-50$  dB, as per ISO 20958 [43]. In Algorithms 2d–2f, the threshold values used in the present study are based on the knowledge of the healthy state of the motor current data. If the motor current data from the healthy motor is unavailable, then a mathematical model of a healthy motor needs to be prepared, as shown by PAL and MOHANTY [39]. Based on the analysis of the current data of healthy motor, the threshold values can be ascertained.

---

**Algorithm 2c.** Detection of the presence of BRBs.

---

1. Calculate  $f_s$  from Algorithm 2a.
2. Calculate  $s$  from Algorithm 2b.
3. The values of pole pass frequencies around the supply line frequency can be observed at:

$$f_{\text{BRBs}} = (1 \pm 2skf_s),$$

where  $k = 1, 2, 3, \dots$

4. Locate  $f_{\text{BRBs}}$  in the 1st column of CS.
  5. Locate the current amplitude in the 2nd column of CS that corresponds to  $f_{\text{BRBs}}$ , denoted as  $\text{CS}_{\text{BRBs}}$ .
  6. Compute the difference in amplitude between  $\text{CS}_{\text{BRBs}}$  and  $\text{Max\_CS}$ , denoted as  $\Delta\text{CS}_{\text{BRBs}}$ .
  7. Set the threshold value of  $-50$  dB for detection of BRBs as per ISO 20958.
  8. **if**  $\Delta\text{CS}_{\text{BRBs}} > -50$  dB **then**
  9.     BRBs exist.
  10.    Set the Boolean value for BRBs as '1'.
  11. **else**
  12.     BRBs do not exist.
  13.    Set the Boolean value for BRBs as '0'.
-

---

**Algorithm 2d.** Detection of the presence of stator faults (SFs).

---

1. Calculate  $f_s$  from Algorithm 2a.
  2. The values of odd harmonics of the supply line frequency can be observed at:
$$f_{\text{SFs}} = (2k + 1) f_s,$$
where  $k = 1, 2, 3, \dots$
  3. Locate  $f_{\text{SFs}}$  in the 1st column of CS.
  4. Locate the current amplitude in the 2nd column of CS that corresponds to  $f_{\text{SFs}}$ , denoted as  $\text{CS}_{\text{SFs}}$ .
  5. Compute the difference in amplitude between  $\text{CS}_{\text{SFs}}$  and Max\_CS, denoted as  $\Delta\text{CS}_{\text{SFs}}$ .
  6. Set the threshold value for detection of SFs as  $-20$  dB for the present motor under study.
  7. **if**  $\Delta\text{CS}_{\text{SFs}} > -20$  dB **then**
  8.     SFs exist.
  9.     Set the Boolean value for SFs as '1'.
  10. **else**
  11.     SFs do not exist.
  12.     Set the boolean value for SFs as '0'.
- 

---

**Algorithm 2e.** Detection of the presence of eccentricity faults.

---

1. Calculate  $f_s$  from Algorithm 2a.
  2. Calculate  $f_m$  from Algorithm 2b.
  3. In a practical scenario, static and dynamic eccentricity coexist together, which is a case of mixed eccentricity. Mixed eccentricity fault tends to excite the sidebands at  $f_m$  around  $f_s$ . Hence, the frequency component indicating the presence of eccentricity fault is represented as:
$$f_{\text{Ecc}} = f_s \pm f_m.$$
  4. Locate  $f_{\text{Ecc}}$  in the 1st column of CS.
  5. Locate the current amplitude in the 2nd column of CS that corresponds to  $f_{\text{Ecc}}$ , denoted as  $\text{CS}_{\text{Ecc}}$ .
  6. Compute the difference in amplitude between  $\text{CS}_{\text{Ecc}}$  and Max\_CS, denoted as  $\Delta\text{CS}_{\text{Ecc}}$ .
  7. Set the threshold value for detection of eccentricity as  $-25$  dB for the present motor under study.
  8. **if**  $\Delta\text{CS}_{\text{Ecc}} > -25$  dB **then**
  9.     Air gap eccentricity exists.
  10.     Set the Boolean value for eccentricity as '1'.
  11. **else**
  12.     Air gap eccentricity does not exist.
  13.     Set the Boolean value for eccentricity as '0'.
-

---

**Algorithm 2f.** Detection of the presence of bearing faults.

---

1. Calculate  $f_s$  from Algorithm 2a.
  2. The frequency component indicating the presence of bearing fault is represented as:
 
$$f_{\text{Brg}} = f_s \pm k f_{\text{Brg-CFFs}}$$
  3. Locate  $f_{\text{Brg}}$  in the 1st column of CS.
  4. Locate the current amplitude in the 2nd column of CS that corresponds to  $f_{\text{Brg}}$ , denoted as  $\text{CS}_{\text{Brg}}$ .
  5. Compute the difference in amplitude between  $\text{CS}_{\text{Brg}}$  and Max\_CS, denoted as  $\Delta\text{CS}_{\text{Brg}}$ .
  6. Set the threshold value for detection of bearing fault as  $-40$  dB for the present motor under study.
  7. **if**  $\Delta\text{CS}_{\text{Brg}} > -40$  dB **then**
  8. Bearing fault exists.
  9. Set the Boolean value for bearing fault as '1'.
  10. **else**
  11. Bearing fault does not exist.
  12. Set the Boolean value for bearing fault as '0'.
- 

**Algorithm 2g.** Detection of the presence of overload torque.

---

1. Calculate the RMS ( $I_{\text{RMS}}$ ) value of the current signal ( $I$ ).
  2. Note the rated current ( $I_{\text{rat}}$ ) as seen in the motor nameplate.
  3. **if**  $I_{\text{RMS}} > I_{\text{rat}}$  **then**
  4. Load torque overload exists.
  5. Set the Boolean value for overload torque as '1'.
  6. **else**
  7. Load torque overload does not exist.
  8. Set the Boolean value for overload torque as '0'.
- 

The presence of CFFs describes the existence of a fault in the motor, and a Boolean value of 1 or 0 is assigned against the type of fault as described in Algorithm 2h. After the fault diagnosis algorithm is processed, the motor health status, denoted by the Boolean value and the current spectrum, is saved in two separate CSV files in the IMC, as depicted in Fig. 3. The names of the report files are denoted by the time during which the motor was analyzed, which helps the plant personnel to track the time of fault creation.

A GCS account is created, and an algorithm is developed for transferring files from IMC to GCS in the Python environment, as described in Algorithm 3. In order to automate the process without any human intervention, windows task scheduler (WTS) is used, which is an inbuilt functionality of Windows 10 OS.

**Algorithm 2h.** Save Boolean and spectrum data.

1. Note the present date and time of analysis.
2. Compile Algorithms 2a–2g.
3. Save the Boolean value in a CSV file corresponding to the fault classified as:

Fault type	Boolean value	
	If fault exists	If there is no fault
Broken rotor bars (BRBs)	1	0
Stator faults (SFs)	1	0
Air gap eccentricity	1	0
Bearing faults	1	0
Load torque overload	1	0

4. Save spectrum data in a CSV file.
5. Name the Boolean and spectrum file based on the present date and time of analysis.

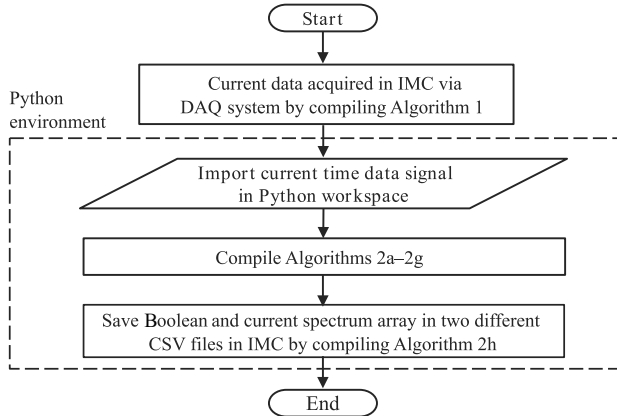


FIG. 3. Flowchart depicting the fault diagnostic algorithm.

**Algorithm 3.** Transfer the Boolean and spectrum CSV files to GCS.

1. The Boolean and spectrum CSV files have been generated on the local computer, as mentioned in Algorithm 2h.
2. Create a bucket in GCS.
3. Move the Boolean and spectrum CSV files from the local computer to GCS.
4. Delete the current time signal from the local computer.

For every motor, the analysis is completed in three stages, as shown in Fig. 4. In the first stage, Algorithm 1 is compiled which triggers the DAQ to record current data from any one of the phases of IM. The second stage involves the execution of Algorithms 2a–2h to carry out fault diagnosis, which generates Boolean and spectrum CSV files called report files. Eventually, in the third stage

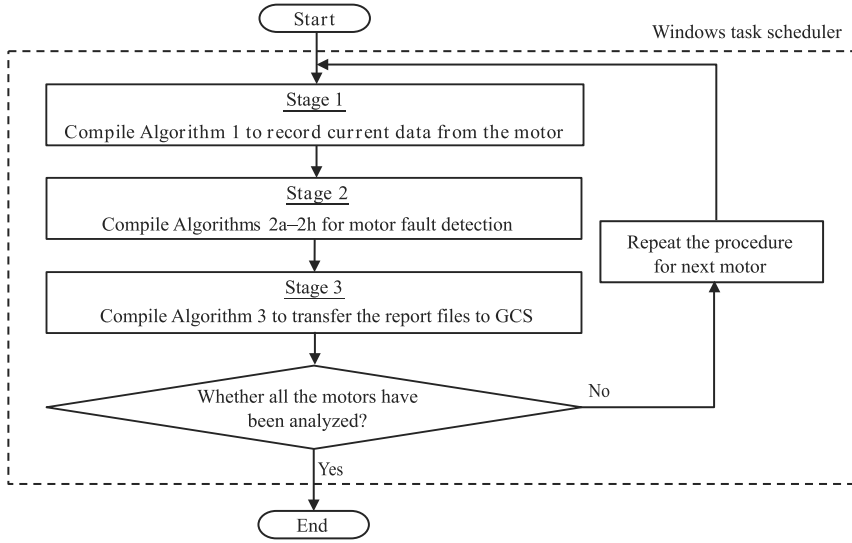


FIG. 4. Methodology applied to automate the fault diagnostic operation.

of WTS, the report files are transferred to GCS by compiling Algorithm 3, from where the plant personnel can access the motor health information. If all five fault types have a Boolean value of 0, then the motor status is declared to be healthy. Therefore, the plant personnel can assess the real-time information of the motor health condition.

### 3. EXPERIMENTAL TEST RIG

Three-phase IMs (M0, M1) and single-phase IMs (M2, M3) were used to experimentally monitor the real-time status of motor health conditions through CPS-oriented fault detection methodology. The motor nameplate details are presented in Table 1. The experimental test rig is illustrated in Fig. 5. The

**Table 1.** Motor nameplate parameters.

Parameter	Unit	M0	M1	M2	M3
Rated power	HP	0.33	1	1.02	1.5
Rated speed	RPM	2850	2830	2700	1440
Rated voltage	V	190	415	230	190
Rated current	A	2	1.65	4.5	8.8
No. of poles	–	2	2	2	4
Rated supply frequency	Hz	50	50	50	50
No. of phases	–	3	3	1	1
Bearing number	–	6203	6004	6203	6203

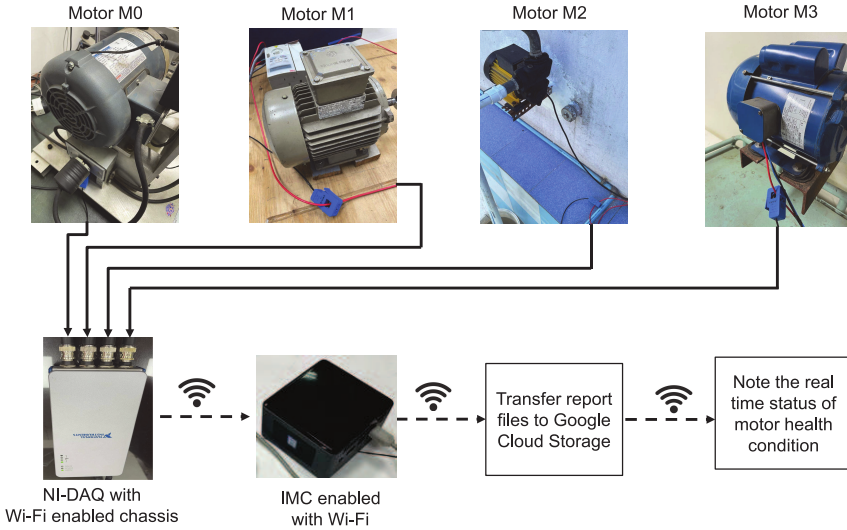


FIG. 5. Experimental setup for the real-time fault diagnosis of IMs.

motor M0 is used as a faulty motor (BRBs), whereas M1, M2, and M3 are healthy motors. The BRBs condition was artificially emulated in motor M0 by drilling three holes through the rotor bars near the end rings. A variable frequency drive was used to operate the motors M0 and M1. A direct online starter was used to operate the motors M2 and M3. A split-core non-invasive current transducer (SCT-013-030) with a sensitivity of 32.4 mV/A was used to measure the instantaneous current drawn by the stator winding. The DAQ system comprises of voltage input module (NI-9215) and a Wi-Fi-enabled chassis (NI-9191). Intel NUC (Next Unit of Computing) was used as an IMC in the present experiment. The digitized current signal data is acquired in IMC across a wireless network by compiling Algorithm 1 developed for the DAQ system. Later, the acquired current data is further processed by passing the current time signal through the fault diagnostic Algorithms 2a–2h. The report files are generated for a motor that consists of a Boolean and spectrum file in CSV format. Eventually, Algorithm 3 is compiled to transfer the CSV files to GCS via Hypertext Transfer Protocol (HTTP) subjected to parallel composite uploads that make the CSV files get uploaded to GCS in the shortest possible time.

#### 4. RESULTS

After the experimental set-up is ready, the WTS is activated, which carries out a three-stage procedure for each motor, as shown in Fig. 4. In the first stage of WTS for motor M0 (motor with BRBs), current data is captured for 20 seconds of time duration by compiling Algorithm 1. During the second stage

of WTS, the recorded current signal in the time domain is then converted into the frequency domain by computing the absolute FFT in a logarithmic scale, which is further subjected to Algorithms 2a–2h. Motor M0 is operated using a variable frequency drive whose supply frequency is detected as  $f_s = 50$  Hz by Algorithm 2a. The motor speed is computed to be 49.65 Hz; hence,  $s = 0.007$  by using Algorithm 2b. By applying Eq. (2.3) and Algorithm 2c, the expected CFFs for BRBs are calculated as  $f_{BRBs1} = 49.3$  Hz and  $f_{BRBs2} = 50.7$  Hz. In the current array (CS), the  $f_{BRBs1}$  and  $f_{BRBs2}$  with the corresponding amplitude values are encountered at (49.3 Hz,  $-40.98$  dB) and (50.7 Hz,  $-45.26$  dB), respectively. As a result, the motor M0 is declared to have BRBs. The report files are generated, which contain the Boolean and spectrum data (until 5000 Hz) in a CSV format and are depicted in Figs. 6 and 7a, respectively. A part of current spectrum data in a graphical format showing CFFs for BRBs of motor M0 is shown in Fig. 7b. Finally, in the third stage of WTS, the report files that are generated for motor M0 are then transferred to GCS by compiling Algorithm 3. Since the IMC has Intel Core i3 processor and 8 GB RAM (random

	A	B	C	D	E
1	Created by Acoustics and Condition Monitoring Lab, IIT Kharagpur				
2					
3	Broken rotor bars	1			
4	Stator winding fault	0			
5	Air-gap eccentricity fault	0			
6	Bearing fault	0			
7	Torque fluctuations	0			
8					

FIG. 6. Boolean report file in CSV format for motor M0.

a)

	A	B	C	D	E
1	Created by Acoustics and Condition Monitoring Lab, IIT Kharagpur				
2					
3	Frequency (Hz)	Log[Current(A)]			
4	0	-77.76283162			
5	0.05	-80.77765562			
6	0.1	-81.05444363			
7	0.15	-75.08410265			
8	0.2	-65.28405997			
9	0.25	-54.64993195			
10	0.3	-57.95820734			
11	0.35	-68.36466027			
12	0.4	-65.12835927			
13	0.45	-66.46126873			
14	0.5	-68.72220411			
15	0.55	-72.46177019			
16	0.6	-66.61215597			
17	0.65	-64.69868428			
18	0.7	-62.9407851			
19	0.75	-69.27924531			
20	0.8	-70.07516044			
21	0.85	-55.58602718			

Spectrum data points upto 5000 Hz

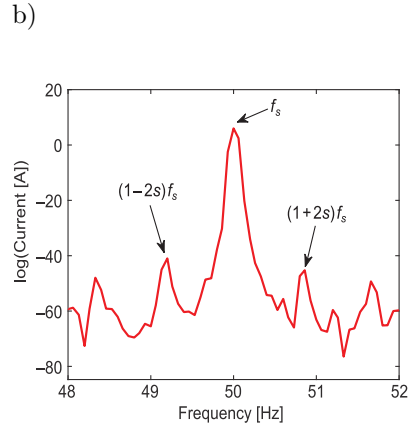
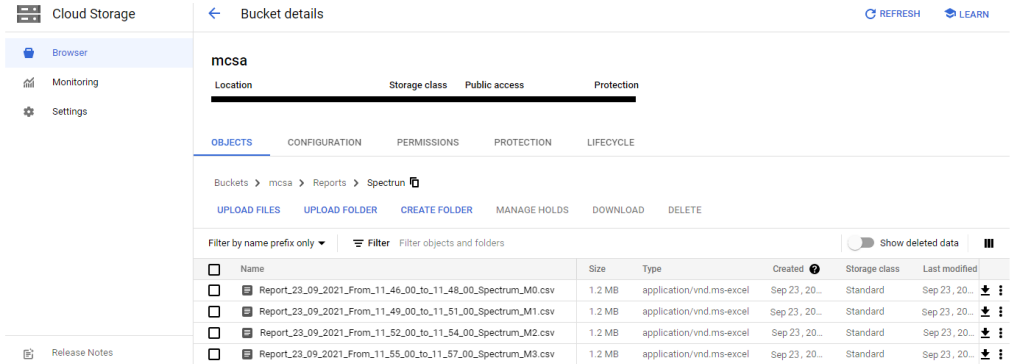



FIG. 7. Spectrum report file in CSV format (a), and part of spectrum plot around supply frequency indicating CFFs for BRBs for motor M0 (b).

access memory), the three-stage procedure of WTS requires 2 minutes for each motor.

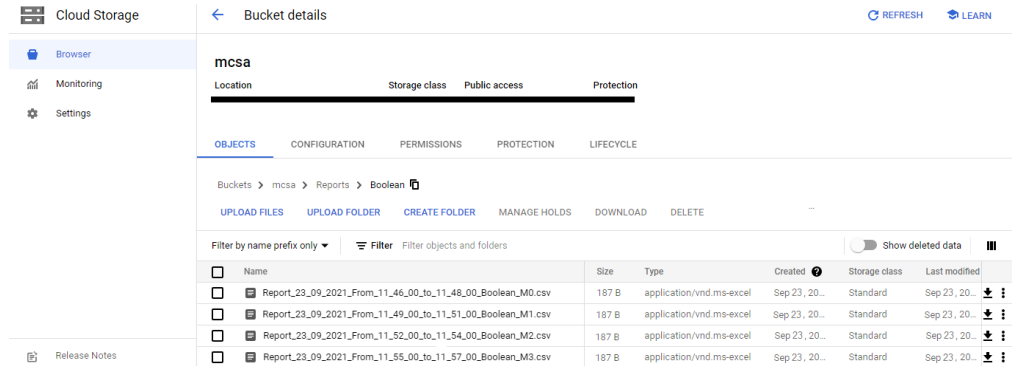
Likewise, the proposed three-stage procedure of WTS is repeated for motors M1, M2, and M3. A bucket is created in GCS where the report files viz. Boolean and spectrum CSV files, for all the motors, are uploaded and shown in Figs. 8 and 9, respectively. The plant personnel can easily access the report files for any motor, from any given location, at any instant of time, which aids in accomplishing the real-time analysis of IMs.



The screenshot shows the Google Cloud Storage interface for a bucket named 'mcsa'. The breadcrumb path is 'Buckets > mcsa > Reports > Spectrun'. The table below lists the uploaded Boolean report files.

Name	Size	Type	Created	Storage class	Last modified
Report_23_09_2021_From_11_46_00_to_11_48_00_Spectrum_M0.csv	1.2 MB	application/vnd.ms-excel	Sep 23, 20...	Standard	Sep 23, 20...
Report_23_09_2021_From_11_49_00_to_11_51_00_Spectrum_M1.csv	1.2 MB	application/vnd.ms-excel	Sep 23, 20...	Standard	Sep 23, 20...
Report_23_09_2021_From_11_52_00_to_11_54_00_Spectrum_M2.csv	1.2 MB	application/vnd.ms-excel	Sep 23, 20...	Standard	Sep 23, 20...
Report_23_09_2021_From_11_55_00_to_11_57_00_Spectrum_M3.csv	1.2 MB	application/vnd.ms-excel	Sep 23, 20...	Standard	Sep 23, 20...

FIG. 8. Boolean report files for motors M0, M1, M2, and M3 uploaded in GCS.



The screenshot shows the Google Cloud Storage interface for a bucket named 'mcsa'. The breadcrumb path is 'Buckets > mcsa > Reports > Boolean'. The table below lists the uploaded Spectrum report files.

Name	Size	Type	Created	Storage class	Last modified
Report_23_09_2021_From_11_46_00_to_11_48_00_Boolean_M0.csv	187 B	application/vnd.ms-excel	Sep 23, 20...	Standard	Sep 23, 20...
Report_23_09_2021_From_11_49_00_to_11_51_00_Boolean_M1.csv	187 B	application/vnd.ms-excel	Sep 23, 20...	Standard	Sep 23, 20...
Report_23_09_2021_From_11_52_00_to_11_54_00_Boolean_M2.csv	187 B	application/vnd.ms-excel	Sep 23, 20...	Standard	Sep 23, 20...
Report_23_09_2021_From_11_55_00_to_11_57_00_Boolean_M3.csv	187 B	application/vnd.ms-excel	Sep 23, 20...	Standard	Sep 23, 20...

FIG. 9. Spectrum report files for motors M0, M1, M2, and M3 uploaded in GCS.

## 5. CONCLUSIONS

This paper presented an integrated framework that shows the significance of real-time analysis of induction motors. The process is based on data transfer across a wireless network, which forms a part of the CPS infrastructure with minimal human intervention. The methodology proposed incorporates the use of a clamp-type current transducer that can be put on one of the phase windings

of input terminals of the motor. The OS of a microcontroller used in embedded systems tends to create random jitters when the sampling frequency of the DAQ unit is set above 500 Hz. Since the range of defect fault frequency is 0–5 kHz, the expected sampling frequency should at least be set at 10 kHz. As a result, an industrial minicomputer is chosen as the best feasible tool to address the criteria of maintaining sampling frequency at 10 kHz. The algorithm for the data acquisition unit is developed in the LabVIEW environment, which is intended to record current data for a time duration of 20 s from each motor. The recorded current data is then passed through an algorithm that aims to investigate the presence of CFFs and assigns a Boolean value as 0 (fault does not exist) and 1 (fault exists) against the fault type. After the analysis is completed, the Boolean and spectrum information is stored in two separate CSV files. The HTTP protocol is implemented to transfer the files to GCS. The naming of the CSV files signifies the time during which the motor was analyzed. In the present article, four motors were used for experimental analysis. The plant personnel can receive the report file of every motor in GCS and assess the real-time information of the motor health condition. The holistic methodology proposed in the presented paper helps the plant maintenance engineers to increase the reliability of the motors under operation by scheduling maintenance tasks.

#### ACKNOWLEDGMENTS

This publication was made possible by the NPRP grant [NPRP13S-0116-200085] from the Qatar National Research Fund (a member of the Qatar Foundation). The statements made herein are solely the responsibility of the authors.

#### REFERENCES

1. CARBONIERI M., BIANCHI N., ALBERTI L., Direct analysis of three-phase induction motor considering rotor parameters' variation and stator belt harmonics effect, *IEEE Transactions on Industry Applications*, **56**(4): 3559–3570, 2020, doi: 10.1109/TIA.2020.2986181.
2. LIU Y., MIAO C., LI X., JI J., MENG D., Research on the fault analysis method of belt conveyor idlers based on sound and thermal infrared image features, *Measurement*, **186**: Article number: 110177, 2021, doi: 10.1016/j.measurement.2021.110177.
3. MOHANTY A.R., *Machinery condition monitoring: Principles and Practices*, Boca Raton, FL, USA: CRC Press, 2014.
4. ABDEL-BASSET M., IMRAN M., Special issue on industrial internet of things for automotive industry – new directions, challenges and applications, *Mechanical Systems and Signal Processing*, **142**: Article number: 106751, 2020, doi: 10.1016/j.ymsp.2020.106751.
5. GEISMANN J., BODDEN E., A systematic literature review of model-driven security engineering for cyber–physical systems, *Journal of Systems and Software*, **169**: Article number: 110697, 2020, doi: 10.1016/j.jss.2020.110697.

6. LEWIS A.J., CAMPBELL M., STAVROULAKIS P., Performance evaluation of a cheap, open source, digital environmental monitor based on the Raspberry Pi, *Measurement*, **87**: 228–235, 2016, doi: 10.1016/j.measurement.2016.03.023.
7. GOUNDAR S.S., PILLAI M.R., MAMUN K.A., ISLAM F.R., DEO R., Real time condition monitoring system for industrial motors, *2015 2nd Asia-Pacific World Congress on Computer Science and Engineering, APWC on CSE 2015*, 1–9, 2015, doi: 10.1109/APWCCSE.2015.7476232.
8. CIVERCHIA F., BOCCHINO S., SALVADORI C., ROSSI E., MAGGIANI L., PETRACCA M., Industrial internet of things monitoring solution for advanced predictive maintenance applications, *Journal of Industrial Information Integration*, **7**: 4–12, 2017, doi: 10.1016/j.jii.2017.02.003.
9. WU D., LIU S., ZHANG L., TERPENNY J., GAO R.X., KURFESS T., GUZZO J.A., A fog computing-based framework for process monitoring and prognosis in cyber-manufacturing, *Journal of Manufacturing Systems*, **43**(1): 25–34, 2017, doi: 10.1016/j.jmsy.2017.02.011.
10. GANGA D., RAMACHANDRAN V., IoT-based vibration analytics of electrical machines, *IEEE Internet of Things Journal*, **5**(6): 4538–4549, 2018, doi: 10.1109/JIOT.2018.2835724.
11. JUNG D., ZHANG Z., WINSLETT M., Vibration analysis for IoT enabled predictive maintenance, *Proceedings – 2017 IEEE 33rd International Conference on Data Engineering (ICDE)*, pp. 1271–1282, 2017, doi: 10.1109/ICDE.2017.170.
12. XENAKIS A., KARAGEORGOS A., LALLAS E., CHIS A.E., GONZÁLEZ-VÉLEZ H., Towards distributed IoT/Cloud based fault detection and maintenance in industrial automation, *Procedia Computer Science*, **151**: 683–690, 2019, doi: 10.1016/j.procs.2019.04.091.
13. MAGADÁN L., SUÁREZ F.J., GRANDA J.C., GARCÍA D.F., Low-cost real-time monitoring of electric motors for the Industry 4.0, *Procedia Manufacturing*, **42**: 393–398, 2020, doi: 10.1016/j.promfg.2020.02.057.
14. FIRMANSAH A., ARIPIHARTA, MUFTI N., AFFANDI A.N., ZAENI I.A.E., Self-powered IoT based vibration monitoring of induction motor for diagnostic and prediction failure, *IOP Conference Series: Materials Science and Engineering*, **588**(1): 012016, 2019, doi: 10.1088/1757-899X/588/1/012016.
15. KUNTHONG J., SAPAKLOM T., KONGHIRUN M., PRAPANAVARAT C., AYUDHYA P.N.N., MUJJALINVIMUT E., BOONJEED S., IoT-based traction motor drive condition monitoring in electric vehicles: Part 1, *Proceedings of the IEEE 12th International Conference on Power Electronics and Drive Systems*, pp. 1184–1188, 2017, doi: 10.1109/PEDS.2017.8289143.
16. CHOUDHARY A., JAMWAL S., GOYAL D., DANG R.K., SEHGAL S., Condition monitoring of induction motor using Internet of Things (IoT), [in:] Kumar H., Jain P. [Eds.], *Recent Advances in Mechanical Engineering. Lecture Notes in Mechanical Engineering*, Springer, Singapore, pp. 353–365, 2020, doi: 10.1007/978-981-15-1071-7\_30.
17. KHAN N., RAFIQ F., ABEDIN F., KHAN F.U., IoT based health monitoring system for electrical motors, *15th International Conference on Emerging Technologies (ICET)*, pp. 1–6, 2019, doi: 10.1109/ICET48972.2019.8994398.
18. ASHMITHA M., DHANUSHA D.J., VIJITLIN M.S., GEORGE G.B., Real time monitoring IoT based methodology for fault detection in induction motor, *Irish Interdisciplinary Journal of Science & Research (IIJSR)*, **5**(2): 72–83, 2021, <https://ssrn.com/abstract=3849600>.
19. ZHANG H.F., KANG W., Design of the data acquisition system based on STM32, *Procedia Computer Science*, **17**: 222–228, 2013, doi: 10.1016/j.procs.2013.05.030.

20. LIBONI L.H.B., FLAUZINO R.A., DA SILVA I.N., MARQUES C.E.C., Efficient feature extraction technique for diagnosing broken bars in three-phase induction machines, *Measurement*, **134**: 825–834, 2019, doi: 10.1016/j.measurement.2018.12.005.
21. LAMIM FILHO P.C.M., PEDERIVA R., BRITO J.N., Detection of stator winding faults in induction machines using flux and vibration analysis, *Mechanical Systems and Signal Processing*, **42**(1–2): 377–387, 2014, doi: 10.1016/j.ymssp.2013.08.033.
22. TANG G.-J., HE Y.-L., WAN S.-T., XIANG L., Investigation on stator vibration characteristics under air-gap eccentricity and rotor short circuit composite faults, *Journal of the Brazilian Society of Mechanical Sciences and Engineering*, **36**(3): 511–522, 2014, doi: 10.1007/s40430-013-0072-4.
23. CHEN R., TANG L., HU X., WU H., Fault diagnosis method of low-speed rolling bearing based on acoustic emission signal and subspace embedded feature distribution alignment, *IEEE Transactions on Industrial Informatics*, **17**(8): 5402–5410, 2021, doi: 10.1109/TII.2020.3028103.
24. GE L., FAN W., XIAO X., GAN F., LAI X., DENG H., HUANG Q., Rolling bearing fault diagnosis method based on improved variational mode decomposition and information entropy, *Engineering Transactions*, **70**(1): 23–51, 2022, doi: 10.24423/EngTrans.1390.20220207.
25. AKBARI A., DANESH M., KHALILI K., A method based on spindle motor current harmonic distortion measurements for tool wear monitoring, *Journal of the Brazilian Society of Mechanical Sciences and Engineering*, **39**(12): 5049–5055, 2017, doi: 10.1007/s40430-017-0762-4.
26. MOHANTY A.R., PRADHAN P.K., MAHALIK N.P., DASTIDAR S.G., Fault detection in a centrifugal pump using vibration and motor current signature analysis, *International Journal of Automation and Control*, **6**(3–4): 261–276, 2012, doi: 10.1504/IJAAC.2012.051884.
27. GARCÍA-SANZ-CALCEDO J., SALGADO D.R., GONZÁLEZ A.G., Drilling projects by tool condition monitoring system (TCMS), *Engineering Transactions*, **64**(4): 555–561, 2016, doi: 10.24423/EngTrans.674.2016.
28. MOHANTY A.R., KAR C., Routray A., An electromagnetic device for fault detection and identification in rotating mechanical components, *The Patent Office Journal*, No. 43/2017, Part 2, Patent No. 288510, 2005.
29. SINGH S., KUMAR A., KUMAR N., Motor current signature analysis for bearing fault detection in mechanical systems, *Procedia Materials Science*, **6**: 171–77, 2014, doi: 10.1016/j.mspro.2014.07.021.
30. BENBOUZID M., A review of induction motors signature analysis as a medium for faults detection, *IEEE Transactions on Industrial Electronics*, **47**(5): 984–993, 2000, doi: 10.1109/41.873206.
31. KAR C., MOHANTY A.R. Vibration and current transient monitoring for gearbox fault detection using multiresolution Fourier transform, *Journal of Sound and Vibration*, **311**(1–2): 109–132, 2008, doi: 10.1016/j.jsv.2007.08.023.
32. BONALDI E.L., DE LACERDA DE OLIVEIRA L.E., BORGES DA SILVA J.G., LAMBERT-TORRESM G., BORGES DA SILVA L.E., Predictive maintenance by electrical signature analysis to induction motors, [in:] *Induction Motors – Modelling and Control*, Esteves Araújo R [Ed.], IntechOpen, 2012, doi: 10.5772/48045.
33. MILJKOVIĆ D., Brief review of motor current signature analysis, *HDKBR INFO Magazin*, **5**(1): 14–26, 2015.

34. SARUHAN H., SARIDEMIR S., ÇIÇEK A., UYGUR I., Vibration analysis of rolling element bearings defects, *Journal of Applied Research and Technology*, **12**(3): 384–395, 2014, doi: 10.1016/S1665-6423(14)71620-7.
35. HUMAYED A., LIN J., LI F., LUO B., Cyber-physical systems security – a survey, *IEEE Internet of Things Journal*, **4**(6): 1802–1831, 2017, doi: 10.1109/JIOT.2017.2703172.
36. BENBOUZID M.E.H., KLIMAN G.B., What stator current processing-based technique to use for induction motor rotor faults diagnosis?, *IEEE Transactions on Energy Conversion*, **18**(2): 238–244, 2003, doi: 10.1109/TEC.2003.811741.
37. PAL R.S.C., MOHANTY A.R., Dynamical modelling of three-phase induction motor with broken rotor bars, *National Conference on Condition Monitoring*, 20–21 September 2019.
38. CRUZ S.M.A., TOLİYAT H.A., CARDOSO A.J.M., DSP implementation of the multiple reference frames theory for the diagnosis of stator faults in a DTC induction motor drive, *IEEE Transactions on Energy Conversion*, **20**(2): 329–335, 2005, doi: 10.1109/TEC.2005.845531.
39. PAL R.S.C., MOHANTY A.R., A simplified dynamical model of mixed eccentricity fault in a three-phase induction motor, *IEEE Transactions on Industrial Electronics*, **68**(5): 4341–4350, 2021, doi: 10.1109/TIE.2020.2987274.
40. PAL R.S.C., MOHANTY A.R., Bearing fault detection in permanent magnet synchronous motors using vibration and motor current signature analysis, *28th International Congress on Sound and Vibration (ICSV)*, 24–28 July 2022.
41. KAR C., MOHANTY A.R., Monitoring gear vibrations through motor current signature analysis and wavelet transform, *Mechanical Systems and Signal Processing*, **20**(1): 158–187, 2006, doi: 10.1016/j.ymssp.2004.07.006.
42. MOHANTY A.R., KAR C., Fault detection in a multistage gearbox by demodulation of motor current waveform, *IEEE Transactions on Industrial Electronics*, **53**(4):1285–1297, 2006, doi: 10.1109/TIE.2006.878303.
43. ISO 20958:2013 *Condition monitoring and diagnostics of machine systems – Electrical signature analysis of three-phase induction motors*, <http://www.iso.org> 2013.

*Received May 27, 2022; accepted version November 26, 2022.*



Copyright © 2023 The Author(s).

This is an open-access article distributed under the terms of the Creative Commons Attribution-ShareAlike 4.0 International (CC BY-SA 4.0 <https://creativecommons.org/licenses/by-sa/4.0/>) which permits use, distribution, and reproduction in any medium, provided that the article is properly cited. In any case of remix, adapt, or build upon the material, the modified material must be licensed under identical terms.